boundary-layer edge is still slightly freestream dependent, the level of eddy viscosity and therefore also the skin-friction coefficient are not. Furthermore, the velocity distribution is consistent with the law-of-the-wall solution.

As a second test case, the RAE2822 airfoil is considered (in particular, case 9 of Ref. 11). Figure 2 compares the pressure and skin-friction distributions of the different models to the experimental results. For the two Wilcox variants the shock is located slightly aft compared to the Cebeci–Smith model and the new $k-\omega$ variant. Similarly as for the flat plate, the TNT $k-\omega$ variant gives lower levels of the skin friction than the two Wilcox variants, and in this case closer to the Cebeci–Smith model and to the experimental values. Most likely, the more aft shock position and the higher skin friction for the two Wilcox variants are a result of higher eddy-viscosity levels (as were seen for the flat plate). This again may be a consequence of the values of ω at the boundary-layer edge being too low. For the TNT $k-\omega$ variant the absence of freestream dependency is shown for the skin-friction coefficient.

IV. Conclusions

The theoretical analysis of TNT interfaces presented in this Note has resulted in a set of constraints that the diffusion coefficients of the $k-\omega$ model (including the cross-diffusion term) should satisfy to resolve the freestream dependency for a model problem. A new set of diffusion coefficients has been chosen that satisfies this set of constraints. Furthermore, these TNT coefficients allow the correct near-wall solution for a constant-pressure boundary layer without the introduction of any blending functions or near-wall modifications, i.e., without introducing the wall distance. Computations for a flat-plate constant-pressure boundary layer and for a two-dimensional airfoil have demonstrated the effective elimination of the freestream dependency at low freestream eddy-viscosity levels, while maintaining the correct near-wall solution.

Acknowledgments

The ENFLOW system has been developed under Contract 01105N awarded by the Netherlands Agency for Aerospace Programmes. To some extent the analysis presented here has been carried out within the framework of the Advanced Viscous Flow Simulation Tools for Complete Civil Transport Aircraft Design (AVTAC) project. The AVTAC project is a collaboration of BAE SYSTEMS, Daimler–Benz Aerospace, Construcciones Aeronauticas SA, Dassault Aviation, Saab, Alenia, German Aerospace Research Center DLR, ONERA, Italian Aerospace Research Center, FFA, and National Aerospace Laboratory NLR. The project is managed by BAE SYSTEMS and is funded by the Commission of European Communities under the Industrial and Materials Technologies initiative (Project BRPR CT97-0555). The author wishes to thank B. Oskam and K. M. J. de Cock for reviewing the manuscript.

References

[1]Wilcox, D. C., "Reassessment of the Scale-Determining Equation for Advanced Turbulence Models," *AIAA Journal*, Vol. 26, No. 11, 1988, pp. 1299–1310.

[2]Wilcox, D. C., *Turbulence Modeling for CFD*, 2nd ed., DCW Industries, Inc., La Cañada, CA, 1998, pp. 119–122.

[3]Menter, F. R., "Influence of Freestream Values on $k-\omega$ Turbulence Model Predictions," *AIAA Journal*, Vol. 30, No. 16, 1991, pp. 1657–1659.

[4]Menter, F. R., "Zonal Two Equation $k-\omega$ Turbulence Models for Aerodynamic Flows," AIAA Paper 93-2906, July 1993.

[5]Wilcox, D. C., "A Two-Equation Turbulence Model for Wall-Bounded and Free-Shear Flows," AIAA Paper 93-2905, July 1993.

[6]Kalitzin, G., Gould, A. R. B., and Benton, J. J., "Application of Two-Equation Turbulence Models in Aircraft Design," AIAA Paper 96-0327, Jan. 1996.

[7]de Cock, K. M. J., "Fully Automatic Navier–Stokes Algorithm for 2D High-Lift Flows," *Fifteenth International Conference on Numerical Methods in Fluid Dynamics*, Vol. 490, Lecture Notes in Physics, Springer-Verlag, Berlin, 1977, pp. 225–231.

[8]Cazalbou, J. B., Spalart, P. R., and Bradshaw, P., "'On the Behaviour of Two-Equation Models at the Edge of a Turbulent Region," *Physics of Fluids*, Vol. 6, No. 5, 1994, pp. 1797–1804.

[9]Boerstoel, J. W., Kassies, A., Kok, J. C., and Spekreijse, S. P., "ENFLOW, a Full-Functionality System of CFD Codes for Industrial Euler/Navier–Stokes Flow Computations," National Aerospace Lab. NLR, TP 96286, Amsterdam, May 1996.

[10]Cebeci, T., and Smith, A. M. O., *Analysis of Turbulent Boundary Layers*, Academic, New York, 1974, pp. 187–191.

[11]Cook, P., McDonald, M., and Firmin, M., "Airfoil RAE 2822—Pressure Distributions and Boundary Layer Wake Measurements," AR 138, AGARD, May 1979.

R. M. C. So
Associate Editor

Numerical Simulation of Unsteady Low-Reynolds-Number Separated Flows over Airfoils

Mahidhar Tatineni* and Xiaolin Zhong†
University of California, Los Angeles, Los Angeles, California 90095-1597

Introduction

LOW-REYNOLDS-NUMBER aerodynamics, in the range of $Re = 5 \times 10^4 - 1 \times 10^6$, is important for a variety of aircraft, ranging from sailplanes and human-powered aircraft to high-altitude unmanned aerial vehicles.[1,2] There has been considerable research, both experimental[3–5] and computational,[6–8] on low-Reynolds-number flows over airfoils.

The flowfield in low-Reynolds-number flows over airfoils is characterized by the presence of separation bubbles, which have a strong influence on the perfomance of the airfoils. The experimental investigations have also considered the unsteady features of low-Reynolds-number flows over airfoils. Leblanc et al.[3] showed that the peak frequencies measured in the velocity spectra for the instability region match the most amplified wave-number and frequency scaling calculated by linear stability theory. The linear evolution of disturbances in the separation bubble was also observed by Dovgal et al.[4] They also detailed the nonlinear interactions of the disturbances and the path to transition.

Low-Reynolds-number separation bubbles include flows in both the subsonic and transonic Mach-number regimes. Drela and Giles[6] and Drela[8] used a viscous-inviscid approach to calculate transonic low-Reynolds-number flows. The simulations used an Euler formulation coupled with an integral boundary-layer formulation, with a transition prediction formulation of e^n type. Their calculations show the strong influence of separation bubbles on the performance of the airfoils. Lin and Pauley[7] used an unsteady, incompressible Navier–Stokes approach to compute low-Reynolds-number flows. Their results show the unsteady nature of the separation bubble and the associated periodic vortex shedding. The dominant frequency was shown to be in agreement with the most amplified frequency from the linear stability analysis, of a mixing layer corresponding to the separated boundary layer.

The present study considers numerical simulation and analysis of low-Reynolds-number compressible flows over airfoils to understand the physics of the separated flows. A detailed linear stability analysis of the separated flow is performed to explain the unsteady nature of the flow. Numerical results show an unsteady vortex shedding process, which is shown through a linear stability analysis to correspond to the instability of the separated boundary layer. The

Presented as Paper 97-1929 at the AIAA 28th Fluid Dynamics Conference, Snowmass Village, CO, 29 June–2 July 1997; received 12 September 1997; revision received 15 June 1999; accepted for publication 13 March 2000.

*Graduate Student. Member AIAA.

†Associate Professor, Mechanical and Aerospace Engineering Department, 420 Westwood Plaza, Engineering IV Building. Member AIAA.

results confirm the linear evolution of disturbances in the separated region. Computations over the Eppler 387 airfoil and the APEX airfoil are the two cases considered. The APEX airfoil was designed at NASA Dryden Flight Research Center for the planned high-altitude flight tests.[2] The airfoil has been designed, using a low-Reynolds-number design code,[8] to operate in the transonic low-Reynolds-number regime. The computations are performed using a time-accurate laminar Navier–Stokes solver. In the computations the equations are transformed from the Cartesian coordinates (x, y, t) into the curvilinear computational coordinates (ξ, η, τ). The flows over the airfoil are computed using a C grid generated using an elliptic grid generator. An implicit second-order finite volume line Gauss–Seidel iteration method[9] is used for the computations. The inviscid terms are computed using the flux-splitting method, and central differencing is used for the viscous terms. The computation involves calculations that are implicit in the η (normal) direction, whereas the ξ (streamwise) direction terms are computed by a line Gauss–Seidel iteration with alternating sweeps in the backward and forward ξ directions. The computations are first-order accurate in time, with the time step being small enough to resolve the time dependence of the solution. The details of the numerical method and its validation are given in our earlier paper.[10]

Results

The time-accurate Navier–Stokes solver is used to calculate unsteady separated low-Reynolds-number flows over the Eppler 387 airfoil and the APEX airfoil. The results for the Eppler 387 airfoil are compared with existing experimental and computational results. A linear stability analysis is performed for the separated boundary layer in both the cases, and the results are compared with the numerical observations.

Eppler 387 Airfoil

Low-Reynolds-number flow over the Eppler 387 airfoil is calculated for the following flow conditions: $Re_\infty = 1 \times 10^5$, $\alpha = 1$ deg, and $M_\infty = 0.2$ using a 314×114 grid. The flowfield in the separated region is found to be unsteady with vortex shedding. The time-averaged results for this case were in good agreement with experimental results. The detailed comparisons were presented in our earlier paper.[10]

The time-accurate numerical solution shows the unsteady separation of the flowfield and the resulting periodic vortex shedding. The vortex shedding process, seen in the unsteady numerical solutions, is visualized in Fig. 1 by using six instantaneous flowfield streamline plots in sequence, corresponding to one time period. The streamline plots from the numerical results also show that the flow in the separated region has a dominant wave number. The instabilities, associated with the separated boundary layer, are analyzed using a linear stability analysis, and the results are compared with numerical results. The time-averaged boundary-layer profile is used as the mean velocity profile. The analysis shows that the boundary layer is unstable for a range of wave numbers. The frequencies and growth rates corresponding to the various wave numbers are plotted in Figs. 2a and 2b. The maximum growth rate occurs at $\alpha^* = 0.1$, where α^* is the nondimensional wave number. The wave number is nondimensionalized as $\alpha^* = \alpha\delta^*$, where $\delta^* = x/(\sqrt{Re_x})$, $Re_x = \rho_\infty U_\infty x/\mu_\infty$. The numerical results are expected to correspond to the most unstable wave number. The instantaneous pressure coefficient distribution obtained from the numerical solutions is used to calculate the dominant wave number in the numerical results. The nondimensional wave number is found to be 0.098, which is within 2% of the value calculated from linear stability theory. Figure 3a shows the frequency spectrum of the unsteady solution at various locations on the surface of the airfoil. For the locations in the separation bubble, the dominant frequency is $\omega^* = 0.039$. This is within 6.5% of the frequency predicted by linear stability theory.

The numerical results also show the generation of subharmonic waves, as shown in Fig. 3a. Figure 3a also shows the subsequent

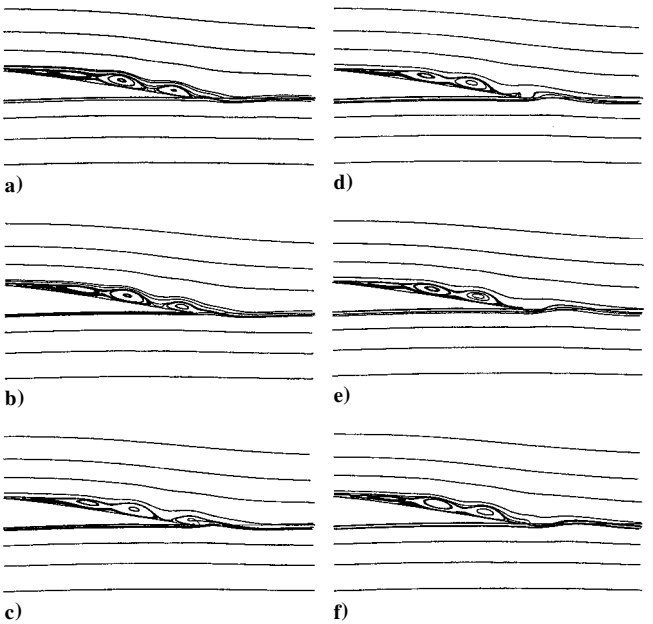

Fig. 1 Flowfield streamline plots in sequence of time, corresponding to one time period, showing the vortex shedding process. Flow over the Eppler 387 airfoil at $M_\infty = 0.2$, $Re_\infty = 1 \times 10^5$, and $\alpha = 1$ deg.

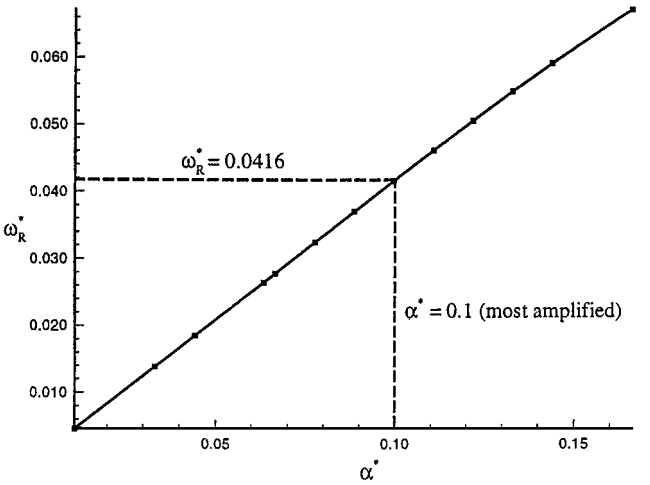

Fig. 2a Variation of the frequency with wave numbers. Results obtained from the linear stability analysis [$\alpha^* = \alpha\delta^*$ and $\omega_R^* = \omega_R(\delta^*/U_\infty)$].

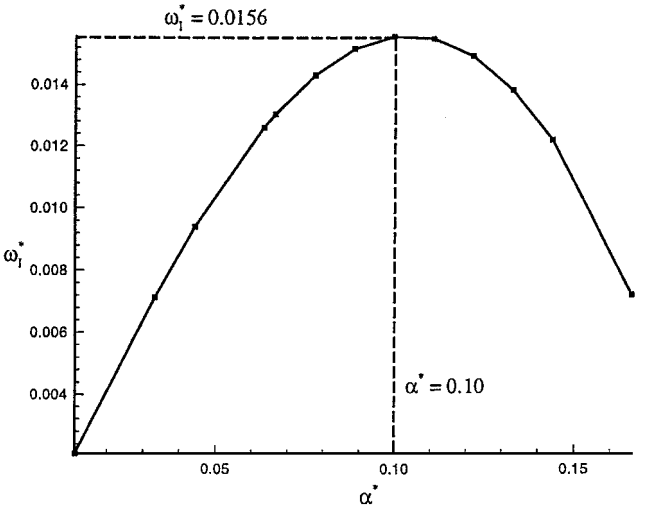

Fig. 2b Variation of the growth rates with wave numbers. Results obtained from the linear stability analysis [$\alpha^* = \alpha\delta^*$ and $\omega_I^* = \omega_I(\delta^*/U_\infty)$]. Flow over the Eppler 387 airfoil at $M = 0.2$, $Re_\infty = 1 \times 10^5$, and $\alpha = 1$ deg.

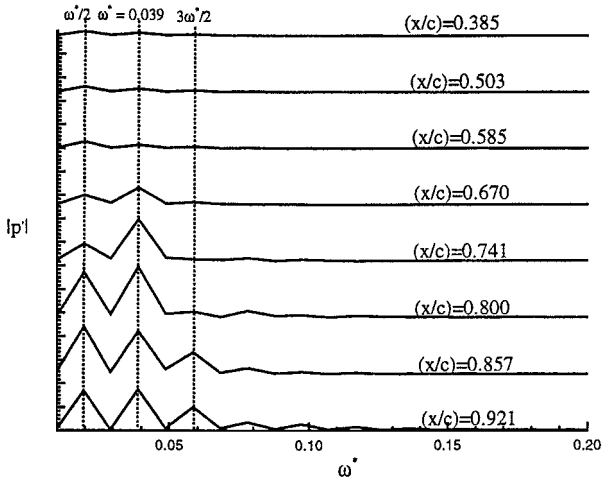

Fig. 3a Frequency spectrum of the pressure disturbance at various locations on the upper surface of the airfoil. Flow over the Eppler 387 airfoil at $M_\infty = 0.2$, $Re_\infty = 1\times10^5$, and $\alpha = 1$ deg.

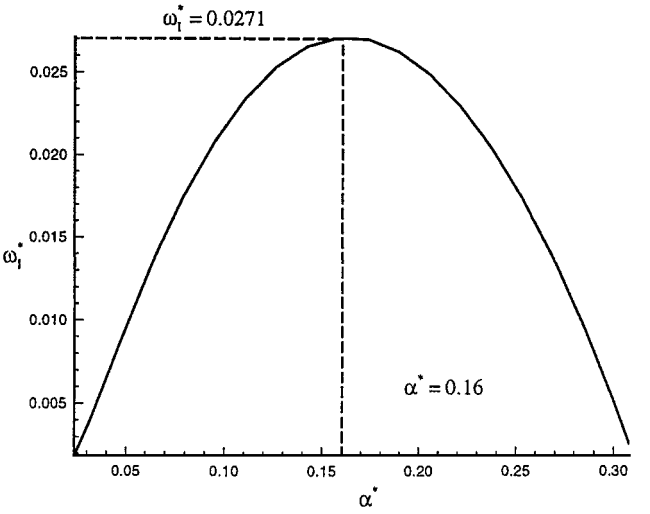

Fig. 4a Variation of the growth rates with wave numbers. Results obtained from the linear stability analysis [$\alpha^* = \alpha\delta^*$ and $\omega_I^* = \omega_I(\delta^*/U_\infty)$].

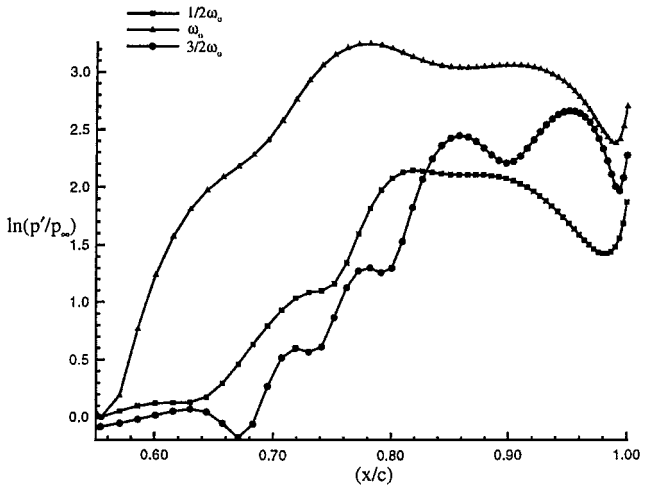

Fig. 3b Growth of disturbance waves along the upper surface of the airfoil. Flow over the Eppler 387 airfoil at $M_\infty = 0.2$, $Re_\infty = 1\times10^5$, and $\alpha = 1$ deg.

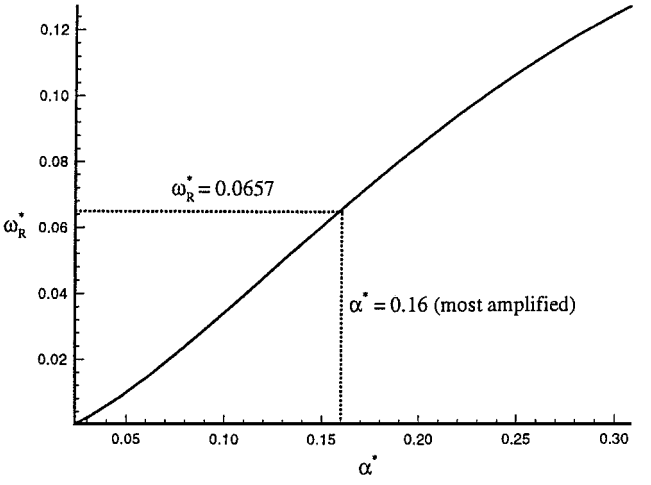

Fig. 4b Variation of the frequency with wave numbers. Results obtained from the linear stability analysis [$\alpha^* = \alpha\delta^*$ and $\omega_R^* = \omega_R(\delta^*/U_\infty)$]. Flow over the APEX airfoil at $M_\infty = 0.5$, $Re_\infty = 2\times10^5$, and $\alpha = 4$ deg.

interaction of two-dimensional fundamental and subharmonic waves. This is expected to lead to nonlinear and three-dimentional effects and, subsequently, transition. This is also illustrated in Fig. 3b, which shows the growth of the different disturbance waves along the surface. Initially, the presence of a dominant frequency is clearly seen. Further along the surface the subharmonic wave begins to grow and interact with the fundamental wave. These numerical results are also consistent with the experimental observations of interactions within the separation bubble by Dovgal et al.[4] Their observations show the initial linear evolution of disturbances, followed by nonlinear interaction of the disturbance waves, leading to transition. In the nonlinear interaction region three-dimensional effects are expected to be important, and a localized three-dimensional calculation will be required to resolve the flowfield.

APEX Airfoil

The flow over the APEX airfoil was calculated for the following freestream conditions: $\alpha = 4$ deg, $M_\infty = 0.5$, and $Re_\infty = 2\times10^5$. A 300×58 grid was used for the computations. The numerical simulations reveal an unsteady vortex shedding process similar to the Eppler 387 case. A linear stability analysis shows that the separated boundary layer is unstable for a range of wave numbers. The growth rates and frequencies are plotted in Figs. 4a and 4b. The most unstable nondimensional wave number from linear stability theory is found to be 0.16. The numerical value for the same is 0.147, which is within 8.5% of the expected value.

Conclusion

Unsteady low-Reynolds-number flows over the Eppler 387 and APEX airfoils have been numerically simulated. Both the studies show the unsteady nature of the separated flow with periodic vortex shedding. The vortex shedding seen in numerical results is found to be caused by the instability of the separated boundary layer. The numerical solution shows the linear evolution of disturbances in the laminar part of the separation bubble. The dominant frequency and wave number seen in the numerical simulations are found to be in agreement with the most unstable wave number and frequency calculated using linear stability theory. The numerical solutions also show that beyond a certain location in the separation bubble there is generation of subharmonics waves and, subsequently, interaction between the fundamental and subharmonic waves. Hence, three-dimensional and nonlinear effects may become important. Further computations are required to ascertain these effects.

Acknowledgments

This research was supported by NASA Dryden Flight Research Center under Grant NCC 2-374. The authors would like to thank

Sean Hu for providing his linear stability analysis code for the analysis in this Note.

References

[1]Lissman, P., "Low Reynolds Number Airfoils," *Annual Review of Fluid Mechanics*, Vol. 15, 1983, pp. 223–239.

[2]Murray, J., Moes, T., Norlin, K., Bauer, J., Geenen, R., Moulton, B., and Hoang., S., "Piloted Simulation Study of a Balloon-Assisted Deployment of an Aircraft at High Altitude," NASA TM 104245, Jan. 1992.

[3]Leblanc, P., Blackwelder, R., and Liebeck., R., "A Comparison Between Boundary Layer Measurements in a Laminar Separation Bubble Flow and Linear Stability Theory Calculations," *Low Reynolds Number Aerodynamics: Proceedings of the Conference*, Springer-Verlag, New York, 1989, pp. 189–205.

[4]Dovgal, A. V., Kozlov, V. V., and Michalke, A., "Laminar Boundary Layer Separation: Instability and Associated Phenomena," *Progress of Aerospace Sciences*, Vol. 30, No. 1, 1994, pp. 61–94.

[5]McGhee, R., Walker, B., and Millard, B., "Experimental Results for the Eppler387 Airfoil at Low Reynolds Numbers in the Langley Low-Turbulence Pressure Tunnel," NASA TM4062, Oct. 1988.

[6]Drela, M., and Giles, M., "Viscous-Inviscid Analysis of Transonic and Low Reynolds Number Airfoils," *AIAA Journal*, Vol. 25, No. 10, 1987, pp. 1347–1355.

[7]Lin, J. M., and Pauley, L. L., "Low-Reynolds-Number Separation on an Airfoil," *AIAA Journal*, Vol. 34, No. 8, 1996, pp. 1570–1577.

[8]Drela, M., "Transonic Low-Reynolds-Number Airfoils," *Journal of Aircraft*, Vol. 29, No. 6, 1992, pp. 1106–1113.

[9]MacCormack, R., "Current Status of Numerical Solution of the Navier Stokes Equations," AIAA Paper 85-0032, Jan. 1985.

[10]Tatineni, M., and Zhong, X., "Numerical Simulation of Unsteady Low-Reynolds-Number Separated Flows over Airfoils," AIAA Paper 97-1929, June–July 1997.

D. S. McRae
Associate Editor

Improved Low-Reynolds-Number k–$\tilde{\epsilon}$ Model

M. M. Rahman* and T. Siikonen†
Helsinki University of Technology, FIN-02015 TKK, Finland

Introduction

THE significance of the linear eddy viscosity k–ϵ model is diminishing due to the deficiency that it cannot accurately predict nonequilibrium flows such as flows with separation and reattachment. The reasoning is most likely to be attributed to the overestimation of k. However, the inclusion of a cross-diffusion term in the ϵ equation may improve the prediction capability of the k–ϵ model, as is experienced by Yoon and Chung[1] for a compression ram flow.

An extension ascribed to the low-Reynolds-number k–$\tilde{\epsilon}$ model of Chien[2] is proposed herein. Essential modifications made in the original Chien (OCH) model include the introduction of the Taylor microscale in the eddy viscosity damping function f_μ and the additional cross-diffusion terms in the k and $\tilde{\epsilon}$ equations, which provoke the level of energy dissipation in nonequilibrium flow regions. The y^+ dependence of the damping function associated with the term that yields a quadratic growth of $\tilde{\epsilon}$ with the wall distance is eliminated by $R_y = \sqrt{(k)}\, y/\nu$. The function multiplying the constant $C_{\epsilon 2}$, which takes the free turbulence into account, is dropped out. Furthermore, the wall singularity is removed by using a physically appropriate timescale that never falls below the Kolmogorov timescale $\sqrt{(\nu/\epsilon)}$.

Received 12 October 1998; revision received 29 February 2000; accepted for publication 2 March 2000.

*Research Scientist, Department of Mechanical Engineering, Laboratory of Applied Thermodynamics, Sähkömiehentie 4.

†Professor, Department of Mechanical Engineering, Laboratory of Applied Thermodynamics, Sähkömiehentie 4.

In essence, comparisons of the model predictions with the experimental and direct numerical simulation (DNS) data for well-studied flows demonstrate that the modified Chien (MCH) model induces a significant improvement over the OCH model.

MCH Model

The proposed model determines the turbulence kinetic energy k and its dissipation rate $\tilde{\epsilon}$ by the following transport equations:

$$\frac{\partial \rho k}{\partial t} + \frac{\partial \rho U_j k}{\partial x_j} = \frac{\partial}{\partial x_j}\left(\left(\mu + \frac{\mu_T}{\sigma_k}\right)\frac{\partial k}{\partial x_j}\right) + \rho P - \rho\epsilon + E_k \tag{1}$$

$$\frac{\partial \rho \tilde{\epsilon}}{\partial t} + \frac{\partial \rho U_j \tilde{\epsilon}}{\partial x_j} = \frac{\partial}{\partial x_j}\left(\left(\mu + \frac{\mu_T}{\sigma_\epsilon}\right)\frac{\partial \tilde{\epsilon}}{\partial x_j}\right) + \left(C_{\epsilon 1}\rho P - C_{\epsilon 2}\rho\tilde{\epsilon} - \rho D e^{-(R_y/80)^2}\right)\Big|\ T_t + E_\epsilon \tag{2}$$

where $\epsilon = \tilde{\epsilon} + D$ and the turbulent production term $P = -\overline{u_i u_j}(\partial u_i/\partial x_j)$. The eddy viscosity and other variables are evaluated as

$$\mu_T = C_\mu f_\mu \rho k T_t, \qquad T_t = \max\left(k/\tilde{\epsilon}, C_T\sqrt{\nu/\epsilon}\right)$$

$$D = 2\nu k\Big|\ y_n^2, \qquad R_y = \sqrt{k}\, y_n/\nu \tag{3}$$

where y_n is the normal distance from the wall and ν represents the kinematic viscosity. The turbulence timescale T_t prevents the singularity at $y_n = 0$ in the dissipation equation. The associated constants are $C_\mu = 0.09$, $C_{\epsilon 1} = 1.44$, $C_{\epsilon 2} = 1.92$, $C_T = \sqrt{2}$, $\sigma_k = 1.0$, and $\sigma_\epsilon = 1.3$.

The near-wall damping function f_μ is taken to be a function of R_λ, defined by

$$f_\mu = 1 - \exp\left(-0.01R_\lambda - 0.0068R_\lambda^3\right)$$

$$R_\lambda = y_n\Big|\ \sqrt{\nu k/\tilde{\epsilon}} = y_n\Big|\ \sqrt{\nu T_t} \tag{4}$$

where $\sqrt{(\nu T_t)}$ is the Taylor microscale. By an analysis of the distinct effects of low Reynolds number and wall proximity, a similar type of eddy viscosity damping function is proposed by Hwang and Lin[3] in their k–$\tilde{\epsilon}$ model. The use of R_λ confronts the singularity at neither the separating nor the reattaching point, in contrast to the adoption of $y^+ = u_\tau y/\nu$, where u_τ is the friction velocity. Consequently, the model is applicable to separated and reattaching flows. In principle, Eq. (4) confirms that the Taylor microscale can be used as an estimate of the near-wall turbulence resolution, physically required to damp out the eddy viscosity.

The extra quantities E_k and E_ϵ in Eqs. (1) and (2) originate from the most extensive turbulent diffusion models for k and ϵ equations derived by Yoshizawa[4] with the two-scale direct-interaction approach using the inertial-range simplification. In the present work, a truncated version is utilized that may be provided with

$$E_k = C_k C_\mu \frac{\partial}{\partial x_j}\left(\frac{k^3}{\tilde{\epsilon}^2}\frac{\partial \tilde{\epsilon}}{\partial x_j}\right), \qquad E_\epsilon = C_\epsilon C_\mu \frac{\partial}{\partial x_j}\left(k\frac{\partial k}{\partial x_j}\right) \tag{5}$$

where C_k and C_ϵ are readjustable model constants. Actually, Eq. (5) signifies the cross-diffusion effects from $\tilde{\epsilon}$ and k in the k and $\tilde{\epsilon}$ equations, respectively. The existence of the cross-diffusion effect from the statistical viewpoint is also pointed out by Leslie.[5] Nevertheless, the contrivance herein is to model Eq. (5) so that optimal results are achievable compared with DNS and experimental data. To receive positive benefits from the numerical reliability and to integrate the condition of inertial-range simplification directly to the solid wall, the cross-diffusion terms are designed as